The Astronomical Journal, 135:907–921, 2008 March doi:10.1088/0004-6256/135/3/907

A PHOTOMETRIC SURVEY FOR VARIABLES AND TRANSITS IN THE FIELD OF PRAESEPE WITH THE KILODEGREE EXTREMELY LITTLE TELESCOPE

Joshua Pepper[1,3], K. Z. Stanek[1], Richard W. Pogge[1], David W. Latham[2], D. L. DePoy[1], Robert Siverd[1], Shawn Poindexter[1], and Gregory R. Sivakoff[1]
[1] The Ohio State University Department of Astronomy, 4055 McPherson Lab, 140 West 18th Ave., Columbus, OH 43210, USA; joshua.pepper@vanderbilt.edu
[2] Harvard-Smithsonian Center for Astrophysics, 60 Garden Street, Cambridge, MA 02138, USA
Received 2007 September 17; accepted 2007 November 28; published 2008 February 5

ABSTRACT

The Kilodegree Extremely Little Telescope (KELT) project is a small aperture, wide-angle search for planetary transits of solar-type stars. In this paper, we present the results of a commissioning campaign with the KELT telescope to observe the open cluster Praesepe for 34 nights in early 2005. Light curves were obtained for 69,337 stars, out of which we identify 58 long-period variables and 152 periodic variables. Sixteen of these are previously known as variable, yielding 194 newly discovered variable stars for which we provide properties and light curves. We also searched for planetary-like transits, finding four transit candidates. Follow-up observations indicate that two of the candidates are astrophysical false positives, with two candidates remaining as potential planetary transits.

Key words: planetary systems – stars: activity

Online-only material: machine-readable table

1. INTRODUCTION

The field of planet searches has grown tremendously in the past several years. One of the techniques for planet detection that has had recent successes is the search for planets transiting their host stars. Transits of bright stars have great scientific potential, giving clues to the internal structure of planets (Guillot 2005), their atmospheric composition (Charbonneau et al. 2002), spin–orbit alignment (Gaudi & Winn 2007), and the presence of rings or moons (Barnes & Fortnoy 2004); see Charbonneau et al. (2007) for a comprehensive review.

To date 18 transiting planets are known. Five of them were discovered first through radial-velocity searches and were then found to be transiting, while the rest were discovered by photometric transit surveys. Of those found using the transit method, five were found by the Optical Gravitational Lensing Experiment (OGLE) survey (Udalski et al. 2002a, 2002b, 2002c, 2003, 2004) but have relatively faint ($V > 16$) host stars. The eight remaining planets orbit relatively bright ($V \leqslant 12$) stars and were discovered by small telescopes with wide fields of view (Alonso et al. 2004; Bakos 2007; Burke et al. 2007; Cameron et al. 2007; McCullough et al. 2006; O'Donovan et al. 2006, 2007).

The Kilodegree Extremely Little Telescope (KELT) project is a wide-field, small-aperture survey for planetary transits of stars with $8 < V < 10$ mag. It is similar to other wide-field transit surveys such as SuperWASP (Pollacco et al. 2006), XO (McCullough et al. 2005), HAT (Bakos et al. 2004), and TrES (Alonso et al. 2004). The justification for the parameters of our survey strategy is described in Pepper et al. (2003), and the instrumentation, performance, and observing strategy are described in Pepper et al. (2007).

In this paper, we report the results of our commissioning observations. These data were used to establish our operational procedures and to build and test the software pipeline. The purpose was not to discover transits with these observations, but rather to use the data to build the analytical tools for use with comprehensive surveys with KELT. The choice to observe the cluster Praesepe was made based on convenience, as an accessible target at the time of commissioning, and the possibility for scientific potential from studying the variable stars in the cluster. The details of the data set analyzed here are not identical to the main KELT survey data, but we can use the observations to test our ability to obtain transit-quality photometry, defined as light curves with low noise, both random and systematic, able to discern astrophysical signals with the timescales and depth of typical planetary transits.

We first briefly review the KELT instrument (Section 2) and describe the Praesepe observations (Section 3). We then discuss the data reduction process (Section 4) with special attention to the problems that affected the data quality (Section 4.1), and assess the photometric precision of the data set (Section 4.6). We explain how we search for variable stars (Section 5) and transit candidates (Section 6). We then list the properties of all variable stars detected and display the light curves of the periodic variables (Section 7), and describe the final set of transit candidates and the observations to confirm their nature (Section 8). We conclude by reviewing the usefulness of this data set and the implications for the full KELT survey (Section 9).

2. INSTRUMENTATION

Here we provide a summary of the full instrumental specifications of KELT that are described in Pepper et al. (2007). The KELT telescope uses an Apogee Instruments AP16E thermoelectrically cooled CCD camera. This camera uses a Kodak KAF-16801E front-side illuminated CCD with 4096 × 4096 9 μm pixels (36.88 × 36.88 mm detector area). It has a gain of 3.6 electrons/ADU, readout noise of ∼15 e^-, and saturates at 16383 ADU (∼59,000 e^-), with very low dark current. The camera is mounted on a Paramount ME Robotic Telescope Mount manufactured by Software Bisque. The Paramount is a research-grade German Equatorial Mount designed specifically for robotic operation with integrated telescope and camera control. For our observations of Praesepe, we use a Mamiya 645 200 mm f/2.8 APO manual-focus telephoto lens with a

[3] Present Address: Physics & Astronomy Department, Vanderbilt University, 6301 Stevenson Center, Nashville, TN 37235, USA.

71 mm aperture. This provides a roughly $9\farcs5$ pix^{-1} image scale and effective $10\fdg8 \times 10\fdg8$ field of view. A Kodak Wratten #8 red-pass filter with a 50% transmission point at ~490 nm is mounted in front of the KELT lens. The effective wavelength of the combined Filter+CCD response function (excluding atmospheric effects) is 691 nm, with an effective width of 318 nm. This results in an effective bandpass that is equivalent to a very broad *R*-band filter.

The KELT telescope is currently operated at the Irvin M. Winer Memorial Mobile Observatory[4] near Sonoita, AZ. The site is located at N 31°39′53″, W 110°36′03″, approximately 50 miles southeast of Tucson at an elevation of 1515 m (4970 feet).

3. OBSERVATIONS

The commissioning campaign targeted a field centered on Praesepe (also called M44 and NGC 2632), an open cluster at a distance of 180 parsecs with an age of 600 Myr, a metallicity slightly above solar, and little to no reddening (An et al. 2007). Several previous studies have examined the cluster population in efforts to determine the stellar luminosity function and to establish overall cluster membership (Jones & Stauffer 1991; Adams et al. 2002), in addition to probing the low-mass end of the stellar population (Chappelle et al. 2005). The amount of interstellar extinction, $E(B-V)$, toward the center of Praesepe is 0.029 mag (Schlegel et al. 1998), corresponding to $A_V = 0.09$ for $R_V = 3.1$.

Our observation were centered on a $10\fdg8 \times 10\fdg8$ field located at J2000 $8^{\rm h}40^{\rm m}06^{\rm s}$, $+19°41'06''$, roughly centered on Praesepe. The observing campaign was conducted every clear night from UTC 2005 February 13 until 2005 April 27, obtaining 5220 images during 34 out of the 74 nights of the run. The observations consisted of 60 s observations repeated throughout the night as long as the cluster was above the horizon, resulting in 100–200 images each night, with a 90 s cadence. The telescope took images on all nights except those with heavy cloud cover or rain. The quality of our observed nights ranged from completely clear to patchy cloud cover. We rely on several steps of the data reduction process to eliminate images with excessive cloud cover, moonlight, or other problems that compromise photometric quality.

The pointing of the KELT telescope was not perfect, with the coordinates of the field center drifting slowly between images throughout the night. The typical intranight drift was ~25′ (~160 pixels) in declination and ~9′ (~60 pixels) in right ascension over the course of many hours. The drift is small compared to the size of the field (<5%), but it has two significant effects on our data. First, the drift causes stars at the edges of the field to enter and exit the camera's field of view during the night, resulting in incomplete light curves for those stars. However, since the image quality is poor at the extreme edges of the field, we simply eliminate stars along the field edges from our sample. Secondly, the drift combines with our image reduction software to cause constant stars in certain parts of the field to spuriously appear as variable candidates. See Sections 4.2 and 5.2 for details of this effect.

4. DATA REDUCTION

For each of the 5220 images of Praesepe, we subtracted the combined dark for that night, and then divided by a flatfield. Images showing large stellar image FWHM or very high (800 ADU) sky levels are eliminated as "bad." These sky levels are mostly caused by clouds. In all, 2083 poor-quality images were eliminated from further analysis. The remaining 3137 images were analyzed using the ISIS image subtraction package from Alard & Lupton (1998); Alard (2000). We adopt the implementation of ISIS described by Hartman et al. (2004). We describe that procedure below, and we note where our procedures differ from those of Hartman et al. (2004).

4.1. Changing FWHM

After initial image processing with ISIS, we found that a large number of variable-star candidates had double-valued light curves, with the amplitude of many sinusoidal light curves being larger on some nights and smaller on others. This variation in amplitude was correlated in time, and appeared to apply mostly to stars in a horizontal zone across the upper part of the chip. We traced the origin of this effect to changing FWHM of the stellar images across our field from night to night. The FWHM does not change significantly horizontally across the field, but it has significant structure in the *Y*-direction, with the FWHM being large (~2.8 pixels) at the top and bottom of the chip, and decreasing linearly toward the middle of the chip in a V-shape, with a minimum FWHM of ~2.0 pixels at about one third of the distance from the top of the chip.

Had the size and shape of this pattern remained constant throughout the observations, it would not have presented a major problem, since ISIS is able to work with a changing FWHM across the field. However, the vertical-axis position of the FWHM minimum changed significantly between different nights, ranging from the middle of the chip to the top edge. That is, the bottom of the V-shape of the FWHM distribution moved up and down the chip over different nights. The position of the FWHM minimum correlated with the change in amplitude of the light curves.

The reason for the double-valued light curves relates to the way ISIS works. ISIS requires a reference image that has the smallest FWHM of all images in the set, since it convolves the reference image with the kernel of each of the individual images. With the changing shape of the FWHM pattern in our data, no single image or set of images has a smaller FWHM across the entire field for all the nights. Any given choice for a reference image will contain a horizontal region for which there are other nights where the stars have smaller FWHM values. Regions with smaller point-spread functions (PSFs) than the reference image on certain nights require deconvolution of the PSFs (i.e. adjusting the stellar images from the reference frame to have smaller PSFs rather than larger). This creates a problem since ISIS works to convolve an image, even with a varying degree across the field, but ISIS is not equipped to correctly *de*convolve an image.

We have not been able to absolutely determine the origin of the time-varying FWHM pattern. We believe it could be related to temperature changes from night to night, which affected the 200 mm lens we used for these observations. Since the problem was not detected until after we stopped using the lens, we were unable to test this hypothesis. Instead, our objective is to mitigate the impact of this effect as much as possible and get the best measurements we can out of the data set.

The procedure we adopted is as follows. We first register the images to the same coordinate system, then divide them into four horizontal sections. For each image section we identify a

[4] http://www.winer.org.

different reference image that has the smallest FWHM out of all images in that section. We then treat the different sections as if they were four separate images, and run each section though the data reduction pipeline with their own reference images to obtain light curves (with an additional subdivision step described in Section 4.2). We also convolve all of the images (but not the reference image) with a Gaussian smoothing function (using a Gaussian with $\sigma = 0.6$ pixels) to slightly broaden the PSFs, and thus ensure that the reference image has a smaller FWHM. With this procedure, we are able to eliminate most of the effects of the time-varying FWHM. We are not able to completely eliminate the effect, which can be seen in the slightly double-valued light curves of some variables (e.g., see plots of KP300133 and EF Cnc in Figure 8, where the scatter in the light curve is more pronounced at the fainter phase of the periodic cycles. Also see the excessive scatter in the light curves of KP407282 and KP118899 in Figure 10, with significant scatter upward when the stars brighten and downward when the stars dim).

4.2. Image Subtraction

We perform image subtraction on each section of the 3137 images with ISIS, as described in Section 4.1. We use a feature of ISIS to further subdivide each section into a grid of subfields, each of which can take on different values for the parameters that are used to convolve the reference image with the kernel for image subtraction. This step is particularly advantageous for large fields of view, in which cloud patterns can be smaller than the size of the field. We subdivide each section into grids from 1×5 to 5×5, depending on the size of the section, and proceed with the image subtraction.

We use DAOPHOT (Stetson 1987) to identify all of the objects in the field of the reference image of each section, yielding a list of 69,337 stars on all four sections. Stars along the image edges have particularly bad light curves, and so we remove all stars within 50 pixels of the edge from further analysis, leaving 66,638 stars for which we generate light curves. The ISIS photometry program calculates the flux from a star and its error in each image. In some situations, such as when the star is located at the edge of the chip, or on the edge of one of the of subregions of the subtracted image, the reported flux and error values are not indicative of the true flux. We clean such points from the data by removing data points where the reported flux or error is unphysically high or low. We also remove the two highest and lowest flux measurements from each lightcurve. Removing such a small number of points should not affect detection of variability or transits, but it does help remove spurious points and reduces the number of false positives when searching for variable sources.

4.3. Astrometry and Matching to Known Sources

We use the *Astrometrix*[5] program to derive astrometric solutions for the reference image, using the Tycho-2 catalog (Høg et al. 2000) to select reference stars. Because of high-order distortions in the corners of the field, we first subdivide the full images into 25 subsections and find separate astrometric solutions for each subimage. The astrometry is good to within an arcsecond, or ~0.1 pixel.

We match our data set to two catalogs. We first match our stars to the Two Micron All Sky Survey (2MASS) catalog (Skrutskie 2006), using a search radius of 9.5 arcseconds or about one KELT pixel. We find that 58,620 out of 66,638 of our KELT stars are in the 2MASS catalog, with 1559 of them matching to more than one 2MASS source.

We also match our star catalog to known members of the Praesepe cluster. We compiled a catalog from the WebDA website, identifying 832 likely cluster members. After matching to the KELT data using a search radius of 9.5 arcseconds, we find matches to 333 Praesepe member stars. However, many of the stars in the WebDA database are too faint for KELT to detect. If we consider only the 210 WebDA sources with known V magnitudes of $6.8 < V < 16.4$, we find matches to 147 stars, although the brighter stars are mostly saturated and unusable in the KELT images.

4.4. Photometric Calibration

Our goal for KELT is to obtain highly precise relative photometry, so we do not attempt to achieve extremely precise absolute photometry. The KELT bandpass is an approximate wide R band. We define a KELT magnitude R_K to which we calibrate our observations, such that

$$R_K \equiv -2.5 \log(\mathrm{ADU\ s^{-1}}) + R_{K,0} \quad (1)$$

where the instrumental ADU s^{-1} is measured using aperture photometry with IRAF, R_K is defined as an approximate KELT R magnitude, and $R_{K,0}$ is the zero-point. We find that the R_K magnitudes are within a few tenths of a magnitude of standard R band photometry, with the uncertainty dominated by the color term. Since we do not have $V - I$ colors for all our stars, we quote R_K, which can be considered equivalent to Johnson R, modulo a color term defined by

$$V = R_K + C_{VI}(V - I), \quad (2)$$

where C_{VI} is the $(V - I)$ color coefficient, and V/I are in the Johnson/Cousins system. Since we do not have previously measured R magnitudes of large numbers of stars in our fields in our magnitude range, we relate R_K to known magnitudes by matching stars from our observations to the *Hipparcos* catalog, selecting only stars with measured V and I colors in *Hipparcos*. We take the mean instrumental magnitude from a set of high-quality images, and match the known magnitudes to the mean instrumental magnitudes, using Equations (1) and (2).

We find a magnitude zero-point of $R_{K,0} = 16.38 \pm 0.06$ mag, and $C_{VI} = 0.55 \pm 0.2$, and that a fiducial $R = 10$ mag star at the field center with $(V - I) = 0$ has a flux of 356 counts per second. Since the *Hipparcos* stars we use to calibrate our data have $(V - I)$ colors mostly between 0 and 1, we expect our calibrations to be less accurate for redder stars. Our observed magnitudes are listed in R_K, which again is equivalent to Johnson R modulo a color term which is typically 0.2 magnitudes, but can range from −0.3 magnitudes for very blue stars to 0.8 magnitudes for very red stars. See Pepper et al. (2007) for additional details about the calibration process.

4.5. Rescaling Errors

One feature of ISIS that has been noted by others is that the formal reported errors tend to be underestimated for brighter stars. Since the errors on individual points are important in the variable selection process, we rescale the errors following the procedure of Kaluzny et al. (1998) and Hartman et al. (2004).

[5] http://www.na.astro.it/~radovich/wifix.htm.

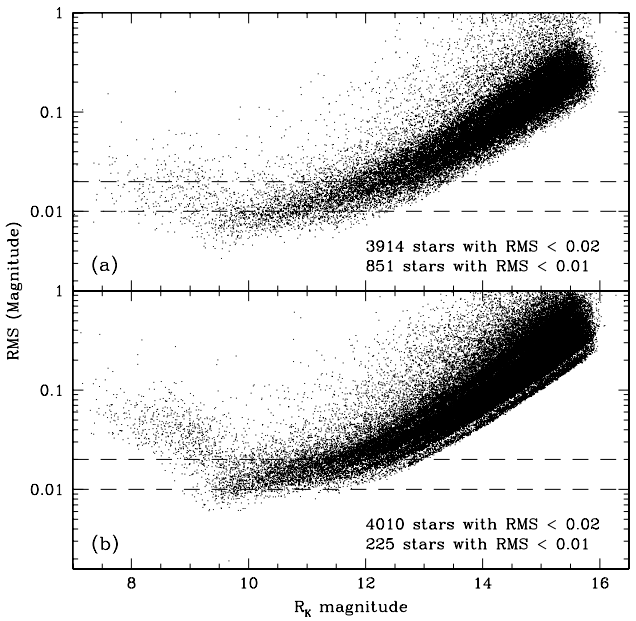

Figure 1. (a) Plot of rms versus R_K magnitude for the 66,638 KELT stars, calculated from 105 observations over the course of one night. (b) Plot of rms for the same stars using all 3137 observations over the full 34 nights. Structure in the plots results from the separate reductions of the four sections of the field to deal with the changes in the FWHM pattern.

We first compute the reduced χ^2 for every star,

$$\chi^2/N_{\rm dof} = \frac{1}{N-1}\sum_{k=1}^{N}\frac{(m_k-\mu)^2}{\sigma_k^2}, \quad (3)$$

where the sum is over N observations, m_k is the instrumental magnitude with error σ_k, and μ is the weighted-average instrumental magnitude. We then plot $\chi^2/N_{\rm dof}$ versus magnitude and fit a curve to the bottom edge of the heaviest concentration of points. We then multiply the formal errors by the square root of the function of that curve, so that the least variable light curves in our data set have $\chi^2/N_{\rm dof}$ close to 1 for all magnitudes.

4.6. Photometric Precision

A common method for describing the photometric precision of transit searches is to plot the magnitude root-mean-squared (rms) values of all the light curves as a function of magnitude. Because of the FWHM changes described in Section 4.1, the long-term photometric precision has been degraded. However, since the intranight FWHM pattern appears to be stable, we plot the overall rms and the rms for one of the nights for all 66,638 stars in Figure 1. Panel (a) of Figure 1 shows the rms plot for a single night of data, while panel (b) shows the rms plot for the full 34 nights of data. The dashed horizontal lines show the 2% and 1% rms limits, which generally define the required sensitivity for detecting Hot Jupiter transits. Two features stand out in these plots. The first is that there are significantly fewer stars with rms $< 1\%$ in plot (b) than plot (a), although there are about the same number of stars in each plot with rms $< 2\%$. This behavior shows that the inter-night systematics, of which we believe the FWHM changes to be the most significant, become most important at the sub-1% level. The second feature to note is the greater rms of stars brighter than $R_K \approx 9$. The light curves of the brightest stars in our sample are dominated by systematic saturation and/or nonlinearity effects that are present during a single night but are more severe over the entire run.

5. VARIABLE SELECTION

Any transit search will yield a data set suitable for detecting variable stars that are unrelated to transiting planets. We implement several cuts to select promising variable star candidates. We first employ the Stetson J statistic (Stetson 1996) to find sources that vary coherently in time. We then remove long-period variables (LPVs) and run a period-search algorithm to find periodic variables based on the $\sigma_{\rm AoV}$ statistic. We run a periodogram filter to remove spurious variables due to aliasing, resulting in a final set of variable star candidates. Finally, we visually inspect the remaining light curves to remove false positives.

5.1. Stetson J Statistic

For each of the 66,638 stars, we compute the Stetson J statistic, using the implementation from Kaluzny et al. (1998). This statistic identifies coherent variable stars by selecting for photometric variations that are correlated in time. After visually examining a number of light curves, we define a cutoff of $J = 0.7$ to select variable candidates, deliberately choosing a liberal cut on J since we have several more tests to filter out non-variables. We eliminate those stars with $R_K < 9$, since the light curves of the brightest stars in our data set are dominated by systematics due to saturation effects. We also eliminate any star that is less than 10 pixels away from stars with $R_K < 9$, since extended wings and bleed trails from the bright stars create false variability. We finally remove any candidate that is less than 13 pixels away from a variable candidate with a higher rms in flux. This eliminates false positives due to constant stars close to true variables. After these cuts we are left with 3430 candidate variable stars.

5.2. Variable Clustering

Among the 3430 variable candidates that pass the cuts described above, most of the stars are clustered around a few of the subsection boundaries, mostly between subsections along the field edges where the fitting parameters vary most, and adjacent subsections closer to the field interior. We assume that all spatial clustering of variables is due to artifacts in the reduction process, and we suspect that the reason for the clustering has to do with how large changes in PSF size and shape across the field affect ISIS.

As described in Section 3, there was an intranight drift in the telescope pointing. One effect of this drift is that stars undergo slight changes in the PSF shape and size during each night. When ISIS convolves the reference image, it uses different parameters for each subsection (see Section 4.2). Subsections at the edges of the field experience the strongest optical distortions due to the wide field, and ISIS has the most difficulty fitting the convolution parameters in those areas. At the edges of those subsections the assumptions used to compute the fitting parameters break down. For stars in those areas, the intranight drift means that any consistently inadequate convolution will show up as photometric variability on timescales comparable to the drift rate.

To eliminate false variability due to this effect, we want to remove any candidates that appear in areas with high spatial clustering. However, these areas are not precisely defined—they result from the combination of the ISIS subsection grid,

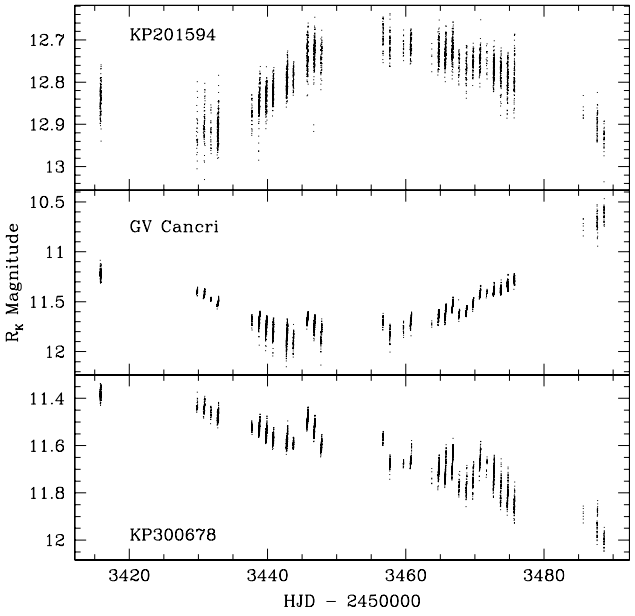

Figure 2. Light curves of three LPVs. We identify KP300603 as semiregular variable star GV Cnc.

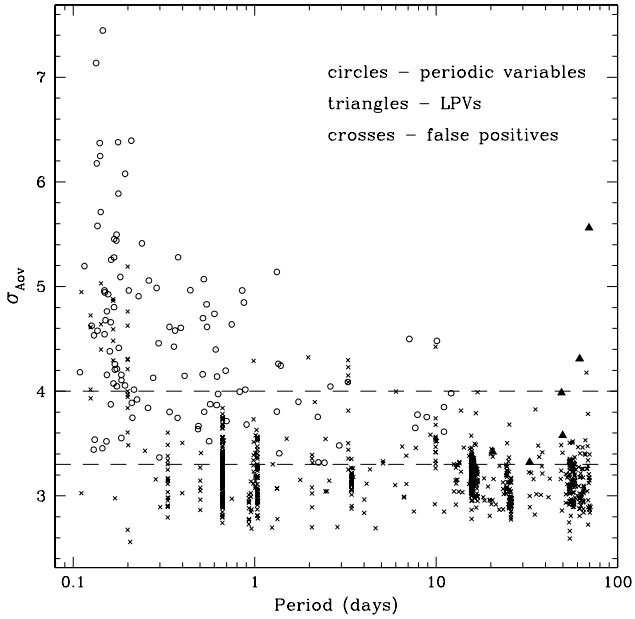

Figure 3. Plot of period versus σ_{AoV} for the 1049 stars left after initial removal of LPVs. The dashed lines show the two cuts on σ_{AoV}. Stars classified as periodic variables are marked by circles and false positives are marked by crosses. As small number of stars that were not removed by the automatic filter for LPVs are determined upon visual inspection to be LPVs, and are marked by triangles.

the direction and speed of the drift, and the nature of the optical distortions. We therefore devised an algorithm to remove from our list any stars that are in clustered areas. We divide the entire field into boxes 100 pixels on a side, and count the number of variable candidates in each box. We perform this process four times, with each grid offset from the previous one by 20 pixels in both the X and Y directions. We thus have four staggered grids with which to measure the clustering of the variable candidates. We classify all candidates that appear in a box with more than two other candidates in any of the grids as spurious and eliminate them from our sample, leaving 1101 variable star candidates.

5.3. Identification of Long-Period Variables

There are some stars that pass the cut on J that do not exhibit periodic variability. Many are long-period variables (LPVs) that show monotonically increasing or decreasing brightness during our campaign, some of which may vary periodically but on timescales longer than our campaign. We identify such objects and remove them from our later analysis, which focuses on identifying periodic variables.

To identify LPVs, we use the method described in Section 4.3 of Hartman et al. (2004), in which a star is defined as an LPV when a parabola fits the lightcurve much better than a horizontal line. We fit a parabola to the 1101 remaining variable candidates and calculate the $\chi^2/N_{\rm dof}$ for the fit, which we call χ^2_{N-3}, along with the $\chi^2/N_{\rm dof}$ for the fit to the mean, χ^2_{N-1} (i.e. a fit to a horizontal line). There are 52 stars for which $\chi^2_{N-3}/\chi^2_{N-1} > 0.8$, and therefore identified as candidate LPVs, which we eliminate from our remaining variable candidate list. We show the light curves of three of our LPVs in Figure 2.

A much smaller fraction of our stars are LPVs (52 out of 66,638 stars, or 0.078%), than the 1535 LPVs out of 98,000 stars, or 1.6%, found by Hartman et al. (2004). We attribute this difference partly to our greater observational time baseline (74 nights versus 30 nights), since we end up classifying stars with periodic behavior in that range as regular periodic variables rather than as LPVs. Also, the Praesepe field is located well out of the Galactic plane, and we therefore expect many fewer background giants than in the field that was observed by Hartman et al. (2004). Since background giants are one of the main types of LPVs (e.g. Mira variables), we would therefore expect fewer LPVs when observing at higher galactic latitudes.

5.4. Periodicity Search

We use the period search algorithm of Schwarzenberg-Czerny (1996) to select periodic variables, adopting the implementation by J. Devor. The Schwarzenberg-Czerny algorithm reports a periodicity likelihood statistic analysis of variance (AoV), and the Devor method analyzes that information to estimate $\sigma_{\rm AoV}$, a measure of the confidence of the light curve's periodicity. We apply the algorithm to the 1049 stars remaining in our catalog after removal of the LPVs.

The plot of the best-fit period P versus $\sigma_{\rm AoV}$ (Figure 3) shows significant aliasing effects at periods that are integer multiples or fractions of one day. We thus need to make further cuts to select the true variables from among our list of candidates. First, we construct three histograms of the 1049 periods in $\log(P)$. Each histogram describes the same set of periods, but the edges of the bins are shifted in $\log(P)$ from the other two histograms by 1/3 of the width of a bin. All objects that appear in bins in any of the three histograms that have more than seven objects in them are rejected, with that number determined empirically by searching for the optimal rejection number while avoiding rejecting too many true variables. Using more than three histograms did not significantly change the set of rejected candidates. Any remaining objects with $\sigma_{\rm AoV} > 3.3$ are retained. To ensure that true variables were not accidentally eliminated by the binning procedure, any stars that have $\sigma_{\rm AoV} > 4.0$ are automatically retained, even if they are caught by the aliasing identification algorithm.

After these cuts, we are left with 182 variable star candidates. We then examine the light curves of the remaining candidates

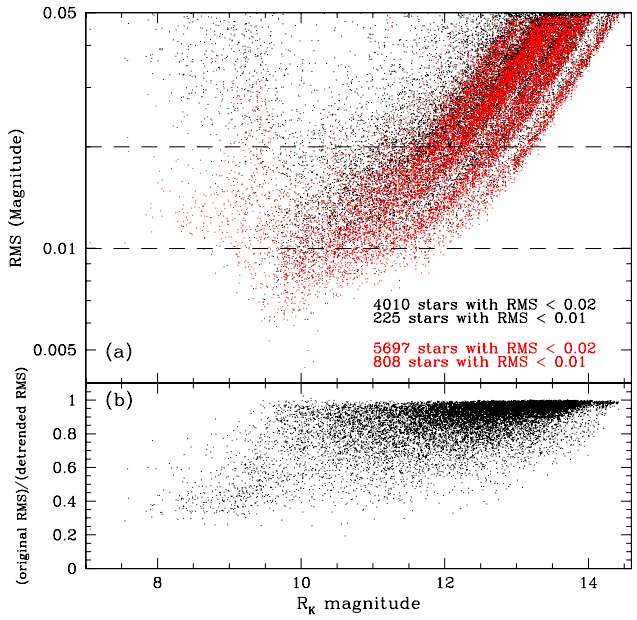

Figure 4. Panel (a) shows the rms plot for 15,012 stars before (black) and after (red) application of SYSREM detrending. Structure in the locations of the fainter stars results from the separate reductions of the four regions to compensate for the changes in the FWHM pattern. Panel (b) shows the change in rms by magnitude.

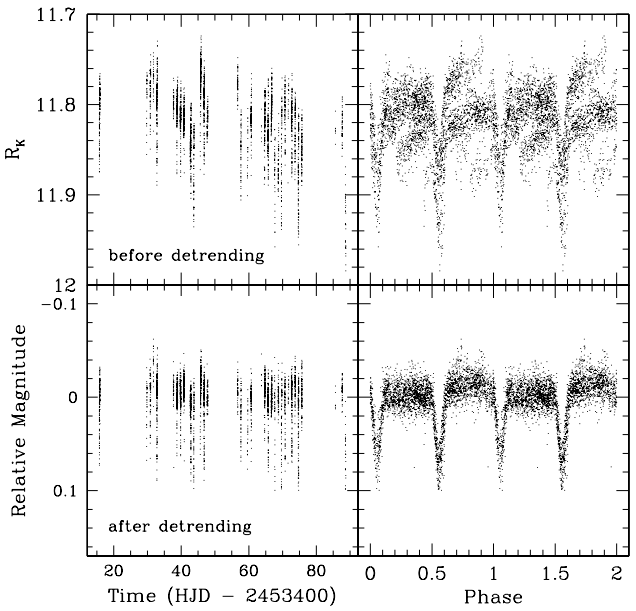

Figure 5. Light curves of the detached eclipsing binary KP102511 (period = 0.5584 days) before and after detrending with SYSREM. The value of σ_{AoV} increased from 3.1 to 4.8.

by hand, and find that 70 of these are false variables, all of which slightly missed the clustering or alias filters. We also find that six of the candidates, all of which have estimated periods longer than 20 days, are in fact LPVs.

6. TRANSIT SEARCH

The primary goal of the main KELT survey is to identify possible planetary transits. We have used the commissioning data set to build our software pipeline and test our data reduction and analysis procedures, without expecting to identify transit candidates in this data set. However, it is still useful to search for transits, since there is still a chance of discovery, and the transit search could also yield interesting variable stars not found through the earlier variable selection method. Furthermore, we would expect to find false positives in the transit search—astrophysical events that look like transits, such as low-mass stars transiting a solar-type star, which would have light curves similar to planetary transits. Finding these events would demonstrate our ability to detect actual transits in the data.

In order to search the data for transits, we take two main steps. The first is to apply a detrending algorithm to reduce or remove a variety of systematics. The second is to run a transit search algorithm over the detrended data and identify transit candidates.

6.1. Detrending

Wide-field transit surveys are susceptible to a number of systematic errors. Observing objects for long stretches of the night requires the telescope to cycle through significant changes in airmass. A wide field of view allows differential cloud patterns to complicate the process of obtaining accurate relative photometry. Temperature changes can affect the optics or detector performance. With so many sources of systematic error, it can be prohibitive to attempt to identify, measure, and compensate for all of these effects. Instead, several methods have been developed to identify all generic systematic effects in data sets of this type. The method we choose to implement is the SYSREM algorithm (Tamuz et al. 2005; Mazeh et al. 2007). In brief, this algorithm identifies and subtracts out linear trends that appear in a large portion of light curves in a given data set.

We apply SYSREM to the KELT light curves that have been reduced using the procedures described in Section 4. Since light curves with very large variations can create problems for detrending programs, and are not useful for the identification of low level systematics, we only apply SYSREM to the 15,012 stars from our data set with rms $< 5\%$. We recalculate the rms for the detrended light curves and display the results in Figure 4. For most of the light curves, detrending improves the rms by about $\sim$10%, although for a few stars, especially toward the bright end, the rms improves by a factor of 3 to 4.

We suspect that the reason that detrending does not improve the rms to a greater degree is related to the FWHM problems described in Section 4.1. Algorithms such as SYSREM are designed to remove linear systematics, but it is probable that the systematic errors caused by the FWHM changes are higher order, and so are not rectifiable by linear detrending. Even so, detrending manages to improve the rms by a small amount, and in some cases works very well, as shown in Figure 5. For the periodic variables we identify with non-detrended rms below 5%, detrending improves σ_{AoV} on average by 10%.

6.2. Transit Selection

To detect transits, we apply a version of the box-fitting least-squares (BLS) transit-search algorithm (Kovacs et al. 2002) implemented Burke et al. (2006). This algorithm cycles through a range of periods and phases searching for a transit-like event and selects the one with the highest significance. For each light curve, we calculate the $\Delta\chi^2$ between a constant flux and the best-fit transit model, the $\Delta\chi^2_-$ for the best-fit antitransit (a brightening rather than dimming), the fraction of $\Delta\chi^2$ that results from a

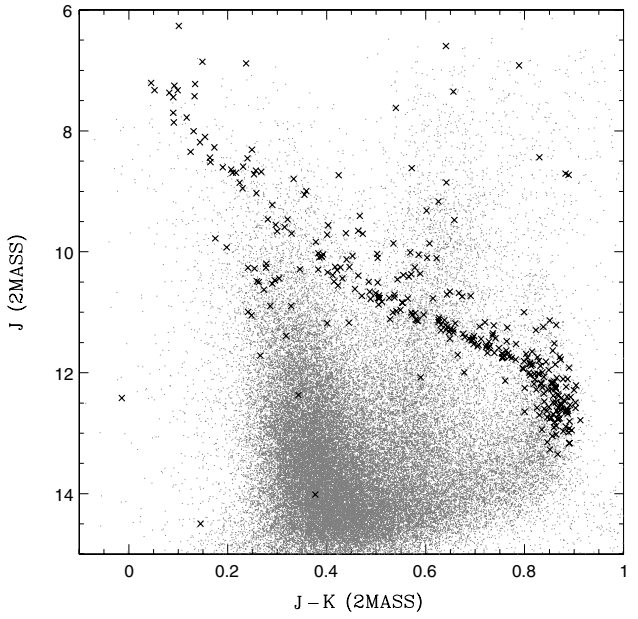

Figure 6. CMD for cluster stars and field stars. Only field stars that match to a single 2MASS source are plotted; all cluster stars have unique 2MASS matches. Dark crosses mark stars listed as members of Praesepe by WebDA.

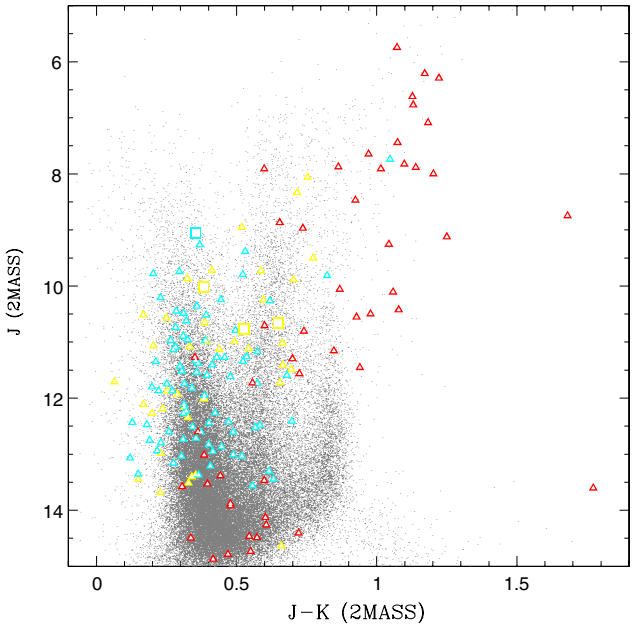

Figure 7. CMD for variable and non-variable stars. Triangles plot the positions of field variables, while squares plot the four cluster variables. Red symbols mark LPVs, blue symbols mark eclipsing binaries, and yellow symbols mark pulsating variables. Only non-variable stars that match to a single 2MASS source are plotted as dots. The eight variable stars that match to more than one 2MASS source are plotted according to the J and K colors of the nearest 2MASS source. The 27 variables that do not match to any 2MASS source are not plotted.

single night f, and the transit period P_t. We then examine five parameters: $\Delta\chi^2$, $\Delta\chi^2/\Delta\chi^2_-$, f, P_t, and the transit depth. We also examine Digital Sky Survey (DSS) images of the stars which have much higher resolution than KELT to check whether the single KELT sources consist of blends of more than one star.

Because of the unique characteristics of this data set, we have elected not to construct a rigorous transit selection algorithm using cuts. Instead we sort the light curves based on each of the five parameters described above, and examine by eye the 100 best light curves identified by each criterion. We classify the light curves as either possible transits, variables, or neither. We find four stars with transit-like behavior that are unblended and that are identified with known 2MASS stars. We also find 38 additional variable stars that were not found with the steps described in Section 5. Of those objects, 31 had $J < 0.7$, which is not surprising since the transit-like signals that BLS searches for would not necessarily show the coherent variations characteristic of a variable star with a large J value. Of the seven other stars, one was eliminated by the cluster-rejection routine, and the remaining six had $\sigma_{\rm AoV} < 3.3$.

7. VARIABLE STARS

After these procedures we are left with 208 variables, which include the 52 LPVs identified in Section 5.3, the 6 LPVs found in Section 5.4, the 112 periodic variables found in Section 5.4, and the 38 periodic variables found in Section 6.2.

7.1. Matching to Known Variables

There are 168 known variables within our field of view combining The General Catalog of Variable Stars (GCVS4.2; Samus & Durlevich 2004) and the New Catalog of Suspected Variable Stars (NSV; Kukarkin et al. 1982),

The magnitudes of the variables are reported in either Johnson V or U, or photographic magnitude p. The range of magnitudes for which we found variables in the KELT data using all the methods described above are $9 < R_K < 16$. Out of the 168 variables, 72 have reported magnitudes outside that range, and an additional 17 are within $15 < V < 16$. We only try to match known variables with reported magnitudes between 9 and 15.

We check whether we detect the remaining 79 variables in our data. We search for KELT counterparts using a matching radius of two pixels (19″) and identify 63 KELT stars that match to known variables. Of the 16 known variables we do not detect, 3 appear either saturated or blended with saturated stars in our data, and 13 do not appear to have counterparts within two pixels of the reported positions, suggesting that the reported positions, proper motions, or magnitudes may be incorrect.

We then compare our list of 208 variables with the 63 detected known variables and find 14 matches. Of the 49 known variables we do not classify as variable through our tests, 5 have counterparts that are either brighter than $R_K = 9$ or blended with a bright star. Another 38 are irregular, eruptive, or unspecified variables, which we would not expect to detect with our periodicity-based search algorithms. Three are eclipsing variables of unspecified type with no periods listed in the catalogs. Upon investigation of their KELT counterparts, no eclipses are seen, indicating that either our observations missed the eclipses, or that the eclipse depths were too small to appear in our data. One is listed as an RR Lyrae variable with no period given, for which the KELT lightcurve shows no periodic variation. The remaining two are eclipsing binaries which are removed in the clustering filter, but can be seen in the KELT light curves. We add those two stars to our list of variables, giving a total of 210.

We thus have KELT light curves for 16 known variables. We find that one KELT LPV is the semi-regular variable GV Cancri. The lightcurve for this object is shown in Figure 2. We find three

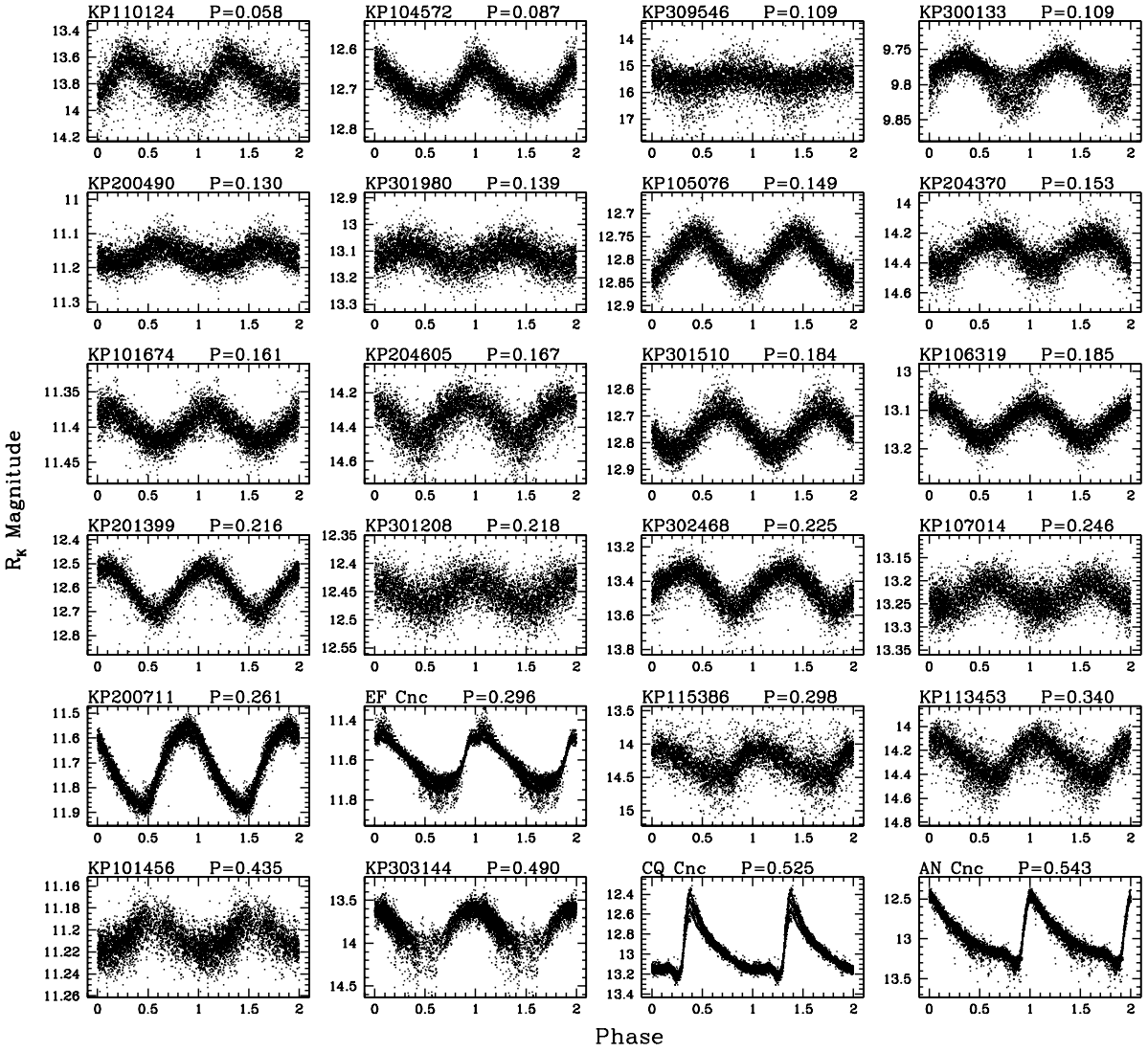

Figure 8. Light curves of pulsating periodic variables identified by KELT, for period range $P < 0.545$ days.

RR Lyrae variables, CQ Cancri, AN Cancri, and EZ Cancri, the first two of which have periods reported in the catalogs that we confirm. One more variable, EF Cancri, is listed as a W UMa contact eclipsing binary, but the light curve, despite the low-quality photometry, appears to indicate that it, too, is an RR Lyrae variable.

We detect six known eclipsing binaries: EH Cancri, GW Cancri, FF Cancri, RU Cancri, NSV 04207, and NSV 04158, in addition to the two eclipsing binaries that were caught by the clustering filter: TX Cancri and RY Cancri. We confirm the reported periods of RY Cancri and TX Cancri, but we find that RU Cancri has a period of 10.0591 days rather than the reported period of 10.172988 days. The remaining variable stars do not have previously reported periods.

The star NSV 04269 is listed as a semiregular variable in the NSV catalog, but our light curve shows it to be an eclipsing binary. The star NSV 04069 is not listed as any variable type; we classify it as an eclipsing binary. Lastly, the star FR Cancri is listed as a BY Draconis variable, consistent with our light curve.

7.2. Variable Star Catalog

We list the properties of our variable stars in Table 1. For each star we list the KELT ID number, mean R_K magnitude, coordinates in right ascension and declination (J2000.0), JHK colors from 2MASS and 2MASS ID for those that matched to 2MASS objects, period (for non-LPVs) in days, type of variable based on our classification, and the GCVS or NSV ID and classification for those that we have identified with previously known variables.

We plot the 2MASS infrared color–magnitude diagram (CMD) for all our stars in Figures 6 and 7. In Figure 6 we show Praesepe cluster members along with all background stars. The cluster members form a coherent main sequence. The background stars form three populations in $J - K$ color. The largest group, at $J - K \sim 0.4$, consists of main-sequence stars. The group at $J - K \sim 0.6$ consists of red giants, and the last group, at $J - K \sim 0.8 - 0.9$, consists of nearby late-type stars, clearly overlapping the same stellar population at the low end of the Praesepe cluster.

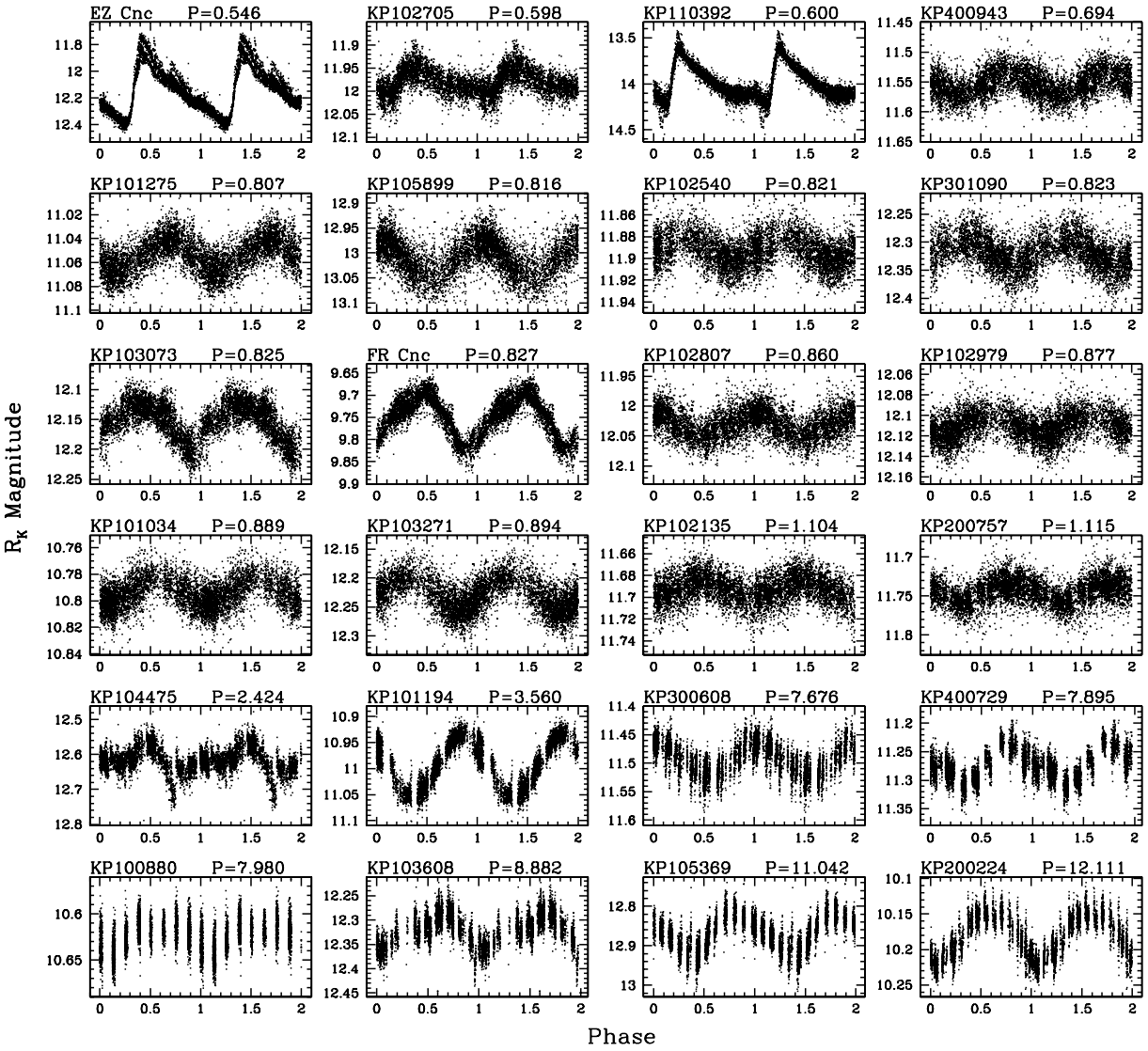

Figure 9. Light curves of pulsating periodic variables identified by KELT, for period range $0.545 < P$ days.

Table 1
Variable Stars Identified in KELT Observations of Praesepe

KELT ID #	R_K	R.A. (J2000.0)	Decl. (J2000.0)	J	H	K	2MASS ID #	Period (days)	KELT Class.	GCVS/NSV ID	GCVS/NSV Class.
KP100169	9.136	133.01755	14.58464	6.212	5.349	5.041	J08520421+1435047	...	LPV	...	...
KP100282	9.495	131.11816	20.20117	9.291	8.881	8.832	J08442835+2012042[b]	1.2065	EB	...	...
KP100305	9.605	133.03393	21.84911	7.440	6.605	6.366	J08520814+2150567	...	LPV	...	...
KP100306	9.606	131.14550	16.28497	7.646	6.826	6.675	J08443491+1617058	...	LPV	...	...
KP100336	9.686	132.50840	17.87422	9.368	8.983	8.838	J08500201+1752271[b]	5.2301	EB	...	...
KP100445[a]	9.930	130.00713	18.99986	9.053	8.767	8.698	J08400171+1859594	0.3828	EB	TX Cnc	W UMa
KP100561	10.149	130.99077	16.71554	7.741	6.932	6.694	J08435778+1642559	1.0438	EB	...	...
KP100626	10.274	135.20934	18.27620	6.291	5.470	5.069	J09005024+1816343	...	LPV	...	...
KP100722	10.408	131.77529	21.03571	8.869	8.321	8.215	J08470606+2102085	...	LPV	...	...
KP100880	10.625	135.54936	16.38090	9.720	9.387	9.308	J09021184+1622512	7.9795	Puls	...	...

Notes.
[a] Members of the Praesepe cluster.
[b] Stars matched to more than one 2MASS source within the 9.″5 matching radius. The 2MASS ID and *JHK* colors in the table are for the closest match within the radius.
(This table is available in its entirety in a machine-readable form in the online journal. A portion is shown here for guidance regarding its form and content)

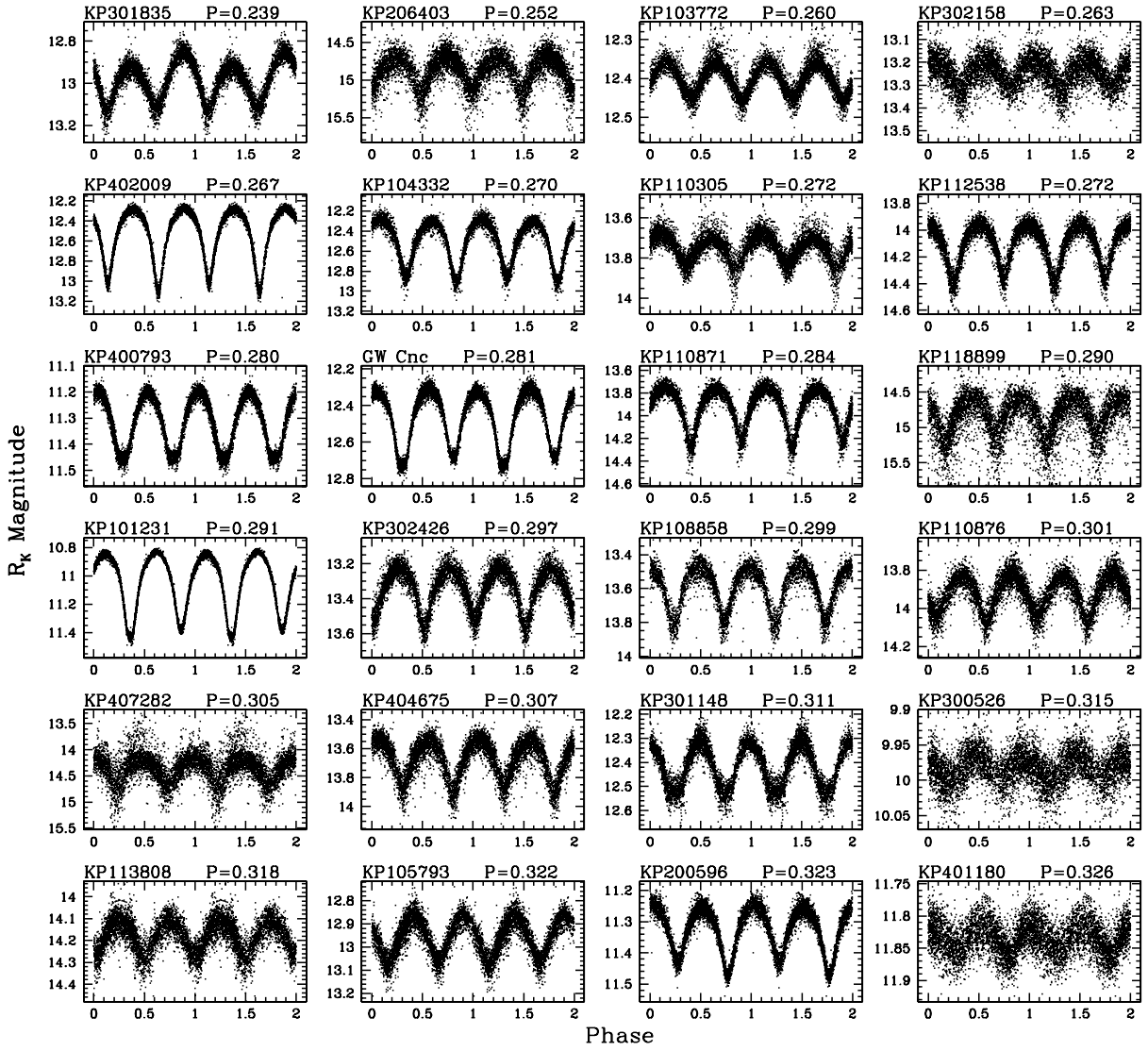

Figure 10. Light curves of eclipsing periodic variables identified by KELT, for period range $P > 0.33$ days.

We plot the light curves of the periodic variables we identify with the methods described above, along with the two previously known periodic variables that missed our cuts. We classify 48 variables as pulsators, and we plot their light curves in Figures 8 and 9. We classify 104 variables as eclipsing binaries, and we plot their light curves in Figures 10–14.

8. TRANSIT CANDIDATES

Using the selection process from Section 6.2, we identify four possible transit candidates. The properties of the four candidates are listed in Table 2, and their light curves are shown in Figure 15. These four light curves all show events with depths of 5% or less and are not blended with nearby stars in DSS images.

Unfortunately, because of the time that has elapsed between the original observations and the final transit selection, calculations of the eclipse ephemerides for the transit candidates are too inaccurate for targeted photometric follow-up. The periods we derive for the candidates are generally accurate to of order 20 s, and since the original observations were taken over two years before the candidates were identified, we do not have ephemerides accurate to within an hour. We therefore use spectroscopic observations to rule out astrophysical false positives.

8.1. Spectroscopic Follow-Up

The four transiting-planet candidates reported in Section 6.2 were followed up spectroscopically using the CfA Digital Speedometer (Latham 1992) on the 1.5 m Tillinghast Reflector at the F. L. Whipple Observatory atop Mount Hopkins, AZ. This instrument has been used extensively for the initial spectroscopic reconnaissance of transiting-planet candidates identified by Vulcan (Latham 2003) and by TrES and HAT (Latham 2007). Single-order echelle spectra centered at 5187 Å were recorded using an intensified photon-counting Reticon detector with a spectral resolution of 8.5 km s^{-1} and typical signal-to-noise ratio of 10–20 per resolution element. After rectification to intensity versus wavelength, the observed spectra were correlated against extensive grids of synthetic spectra drawn from a library calculated by Jon Morse using Kurucz (1992) model atmospheres and codes. This allowed us to estimate the

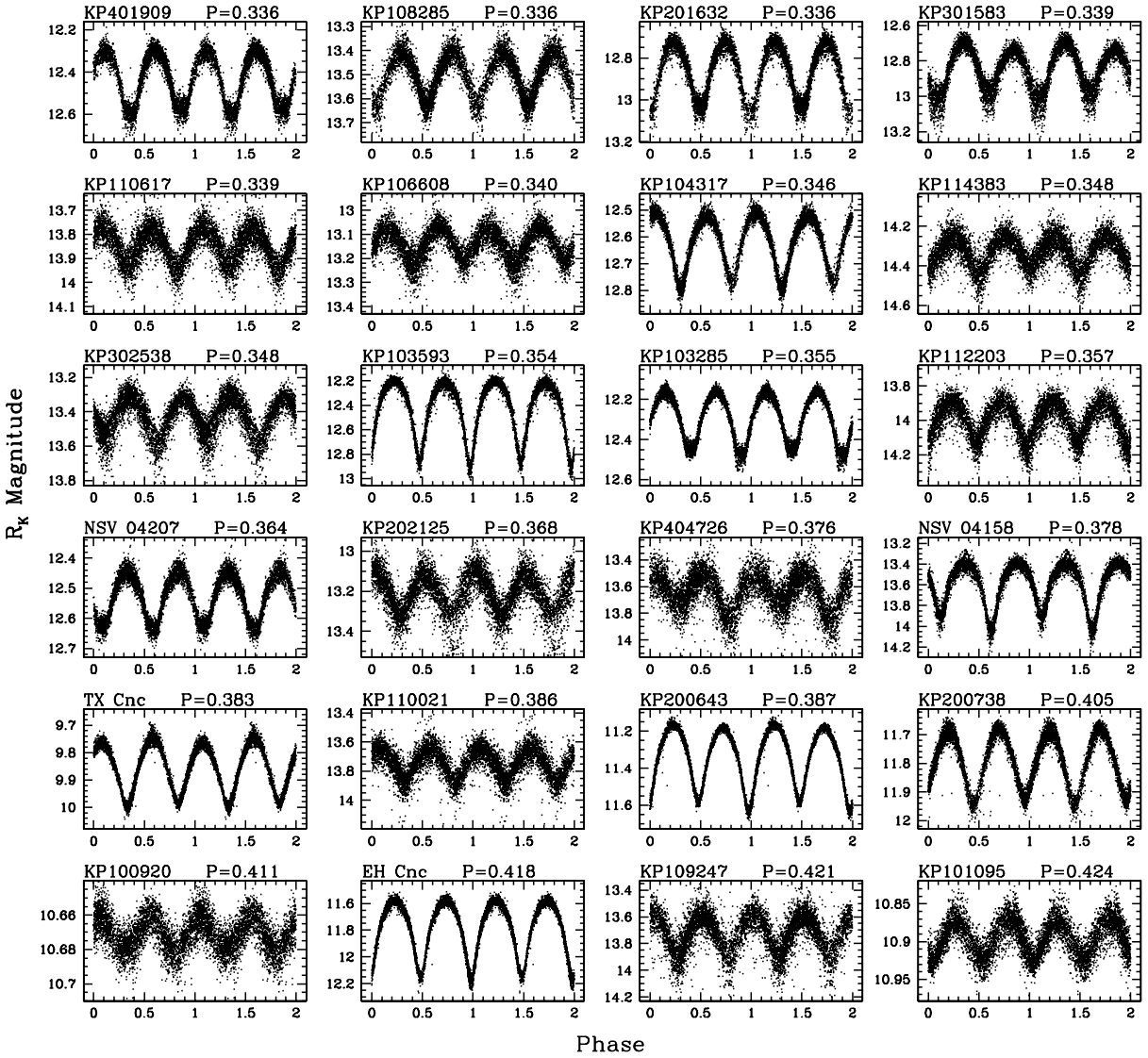

Figure 11. Light curves of eclipsing periodic variables identified by KELT, for period range $0.33 < P < 0.43$ days.

Table 2
Properties of KELT Transit Candidates

KELT ID	2MASS ID	R.A. (J2000.0)	Decl. (J2000.0)	R_K mag	$J - K$ (2MASS)	Period (days)
KP102662	J08525435+1447557	133.22647	14.79883	11.96	0.31	1.8558
KP102791	J08465697+1603190	131.73742	16.05529	12.02	0.30	3.0227
KP200924	J08362287+2045100	129.09531	20.75279	12.05	0.57	0.6246
KP103126	J08530235+2045045	133.25982	20.75127	12.17	0.38	0.4984

effective temperature and surface gravity of the star, assuming solar metallicity, as well as the rotational and radial velocities. For the initial spectroscopic reconnaissance we normally obtain at least two spectra, so that we can look for velocity variations down to the level of about 1 km s^{-1} for slowly-rotating solar-type stars.

In the case of KP200924 the first CfA observation revealed that this candidate has a composite spectrum. Plots of the one-dimensional correlation functions clearly show two peaks corresponding to the two stars in a double-lined spectroscopic binary, with a velocity separation of about 200 km s^{-1} and rotational broadening of about 65 km s^{-1}. This must be a grazing eclipsing binary.

For KP102791 we obtained 14 CfA spectra spanning 88 days. The spectroscopic analysis yielded an effective temperature of $T_{\rm eff} = 7000$ K, a surface gravity of $\log(g) = 4.5$ cm s^{-2}, and rotational velocity of $V_{\rm rot} = 27.5$ km s^{-1}. The 14 radial velocities, listed in Table 3, allowed us to derive a single-lined spectroscopic orbit with period $P = 3.0227 \pm 0.0011$ days, eccentricity $e = 0.033 \pm 0.026$, orbital semi-amplitude $K = 64.9 \pm 1.0$ km s^{-1}, and mass function $f(m) = 0.00856 \pm 0.00039$ solar masses; see Figure 16. Note that the spectroscopic

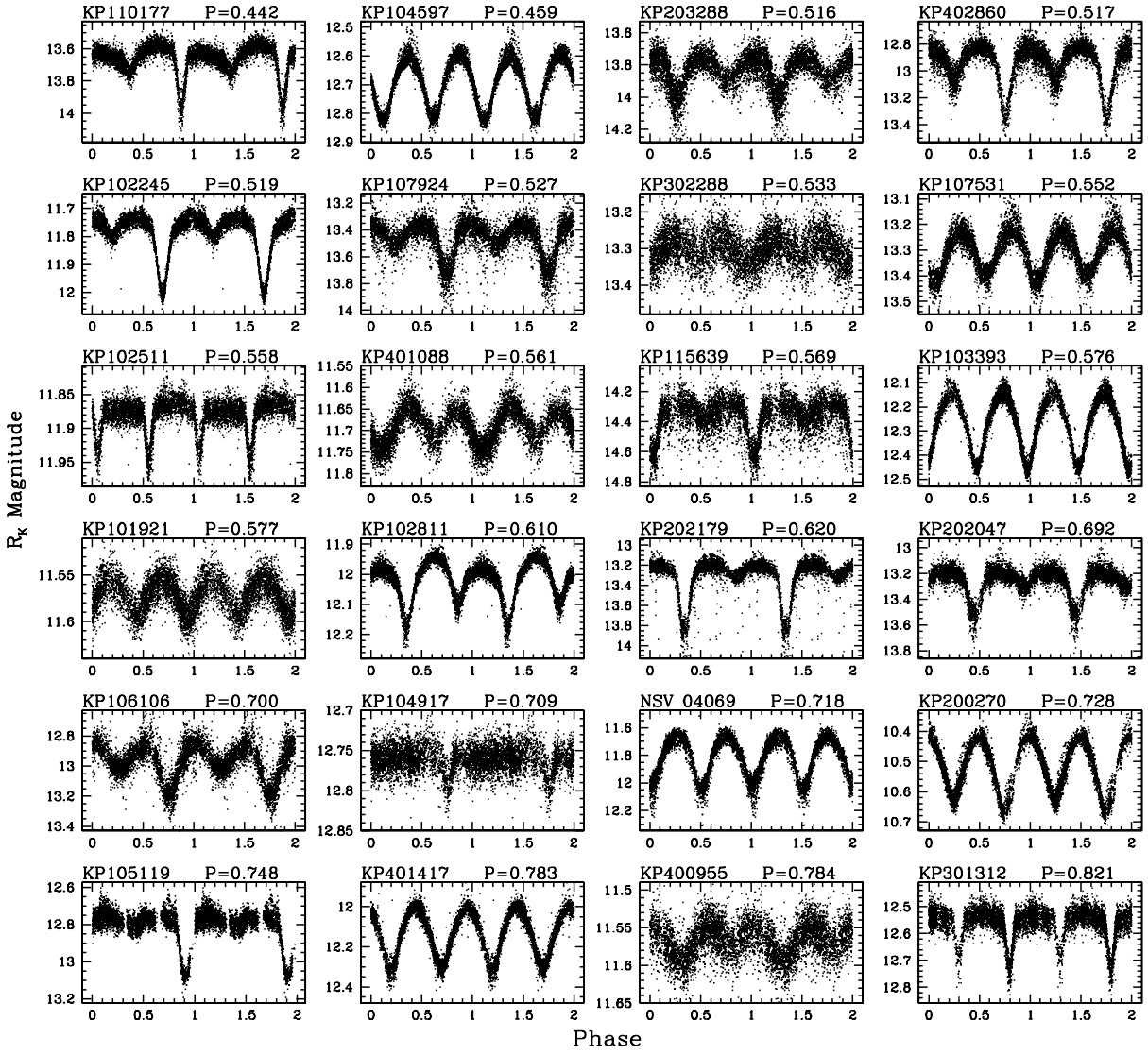

Figure 12. Light curves of eclipsing periodic variables identified by KELT, for period range $0.43 P < 0.83$ days.

Table 3
Radial Velocities for KP102791

HJD (days)	$V_{\rm rad}$ (km s^{-1})	$\sigma(V_{\rm rad})$ (km s^{-1})
24454108.8575	34.95	1.91
24454127.7863	37.87	1.77
24454135.8422	8.25	1.83
24454137.8649	−70.69	1.84
24454162.7826	−27.46	1.92
24454165.7497	−28.09	1.82
24454166.7061	58.08	1.36
24454190.7266	57.66	1.41
24454191.6968	−19.43	1.89
24454192.6877	−58.26	2.43
24454193.7257	52.89	1.64
24454194.6724	−11.43	1.82
24454195.7780	−50.40	1.71
24454196.6919	49.67	2.12

period is twice the photometric period, which often happens when the secondary eclipses look similar to the primary eclipses. The eccentricity is indistinguishable from circular, suggesting that the orbit has been circularized by tidal forces. Thus, it is not unreasonable to assume that the rotation of the two stars has been synchronized and aligned with the orbital motion. In this case the observed spectroscopic line broadening can be used to estimate the radius of the primary star, which comes out to about 1.6 solar radii. This in turn implies that the primary has not evolved very much, which is consistent with the surface gravity derived from the spectra. Adopting a mass of 1.5 solar masses for the primary, the mass of the unseen secondary implied by the mass function is about 0.75 solar masses. The ephemeris for future primary eclipses based on just the radial velocity data is $2454170.445 \pm 0.069 + (3.0227 \pm 0.0011) \times E$. Observations with KeplerCam on the 1.2 m reflector at the Whipple Observatory revealed an ingress starting at heliocentric Julian date 2,454,165.84. Unfortunately the event started 6 h later than predicted by the photometric ephemeris available at that time from data that were already two years old, and the ingress was still in progress and already 0.025 magnitudes deep when the telescope reached its pointing limits. It turns out that this particular transit event must have been a secondary eclipse,

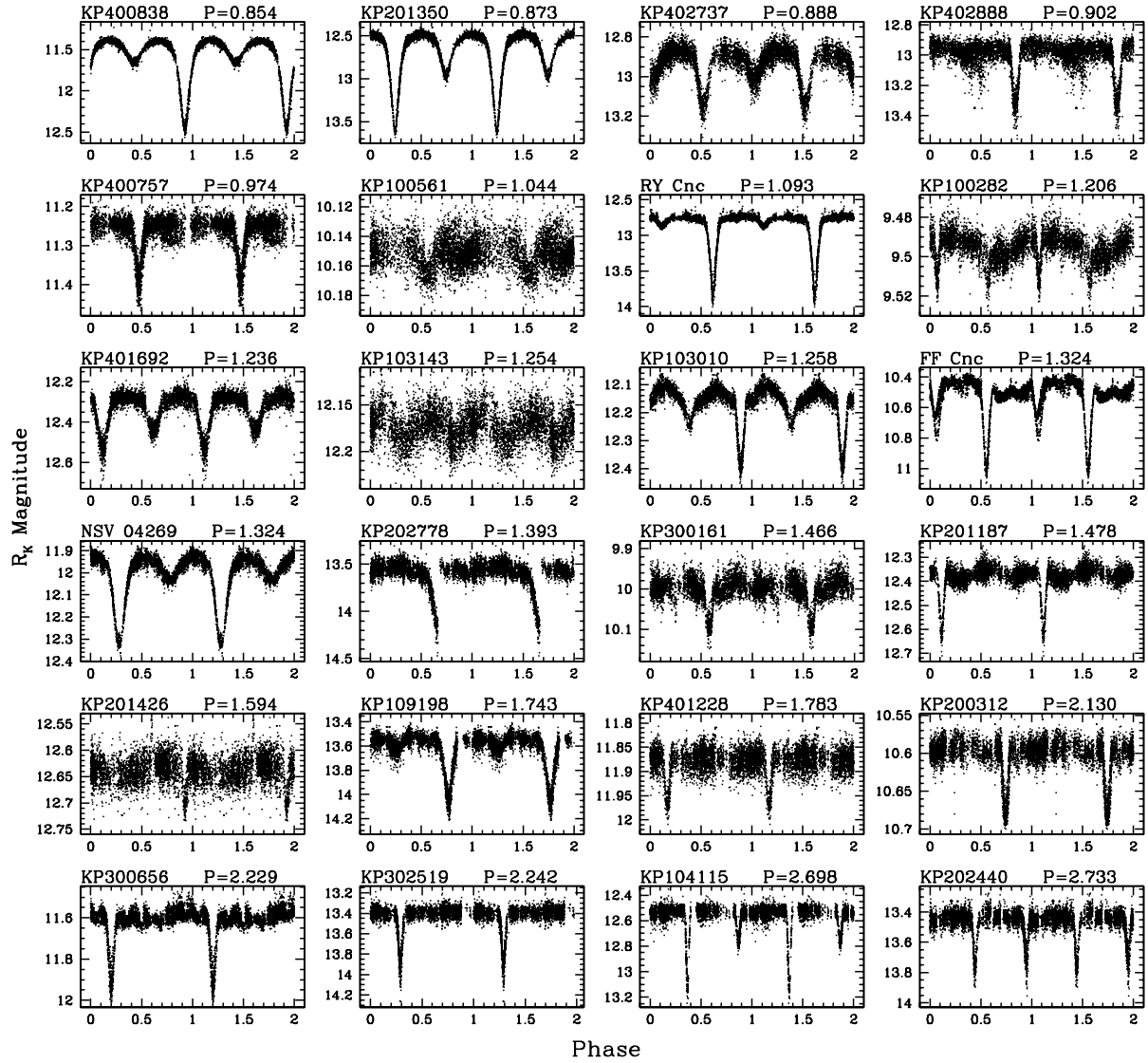

Figure 13. Light curves of eclipsing periodic variables identified by KELT, for period range $0.83 < P < 3$ days.

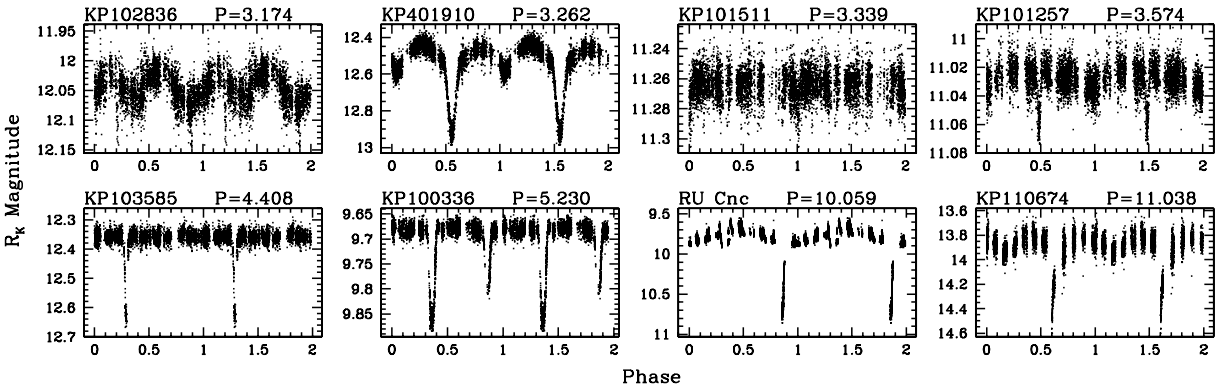

Figure 14. Light curves of eclipsing periodic variables identified by KELT, for period range $P > 3$ days.

with its center almost exactly 1.50 cycles after the spectroscopic epoch for primary eclipses quoted above.

For KP102662 we obtained five CfA spectra spanning 33 days. The spectroscopic analysis yielded $T_{\rm eff} = 6500$ K, $\log(g) = 4.5$ $V_{\rm rot} = 3.5$ km s^{-1}, and mean radial velocity $\langle V_{\rm rad}\rangle = -20.83 \pm 0.37$ km s^{-1} rms. The χ^2 probability that the observed velocity residuals are consistent with Gaussian errors and constant velocity is $P(\chi^2) = 0.82$, so if the transit-like light

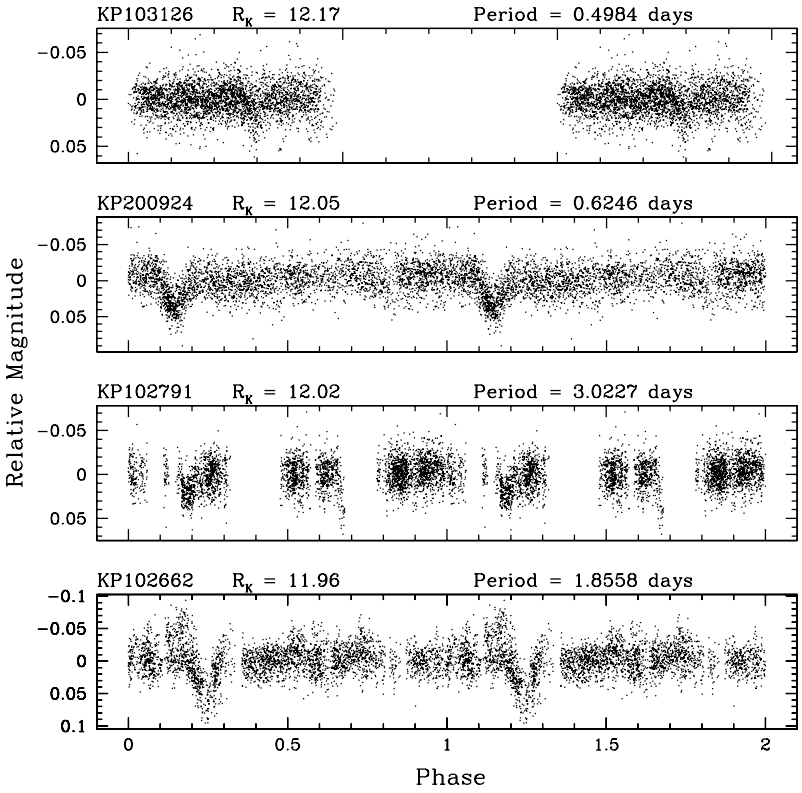

Figure 15. Light curves of the four best transit candidates.

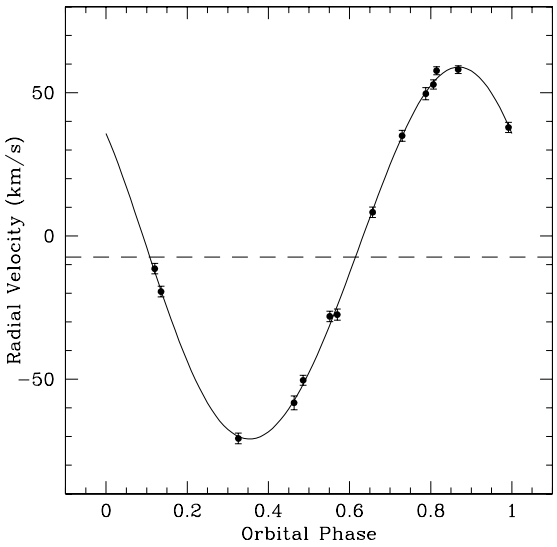

Figure 16. Spectroscopic orbit of transit candidate KP102791, with a period of 3.0227 ± 0.0011 days. The amplitude of the orbit clearly indicates that the companion is a stellar companion and not a planet. This object turns out to be an eclipsing binary with a 1.5 $M_\odot$ primary and a 0.75 $M_\odot$ secondary.

curve observed for the visible star in this system is caused by an orbiting companion, the companion mass must be less than just a few Jupiter masses. On this basis KP102662 survives as a viable transiting planet candidate. However, the transit light curve looks V-shaped and rather too deep to allow a Jupiter-sized planet. Nevertheless, this candidate deserves further follow-up observations. Obtaining a high-quality lightcurve would probably prove to be time consuming, because the ephemeris is based on data that are already two years old, so highly precise radial velocities may be the best way to proceed.

For KP103126 we obtained six CfA spectra spanning 58 days. The spectroscopic analysis yielded $T_{\rm eff} = 6250$ K, $\log(g) = 4.5$ cm s^{-2}, $V_{\rm rot} = 0.5$ km s^{-1}, $\langle V_{\rm rad} \rangle = -11.49 \pm 0.79$ km s^{-1} rms, and $P(\chi^2) = 0.035$. The velocity residuals are a bit larger than expected, but still consistent with an orbiting companion that is no more than several Jupiter masses. Thus this candidate also survives as a viable transiting-planet candidate, one that might reward highly precise radial-velocity observations.

9. CONCLUSIONS

This paper has presented an analysis of the KELT commissioning data, consisting of a 74-day campaign toward the Praesepe open cluster. We obtained light curves for over 66,000 stars, and identified 210 variable stars, of which 194 were not previously known as variable.

We have also searched for planetary transits, finding four transit candidates. Follow-up observations have ruled out two of the candidates as being non-planetary in origin, while two remain as possible planetary systems. This data set has served as the testbed for developing the variable and transit search algorithms that will be used to analyze data from the main KELT survey, and has demonstrated the ability of KELT to detect signals at the level of precision of transiting planets.

We would like to thank the many people who have helped with this research, including Scott Gaudi, Mark Trueblood, and Pat Trueblood. We would also like to thank Marc Pinsonneault and Deokkeun An for discussions about cluster and stellar properties. We would like to thank the authors of several programs

used for this research, including W. Pych for the program to determine FWHM, Christopher Burke for the implementation of the BLS algorithm, and G. Pojmanski for the `lc` program for analyzing light curves. This work was supported by the National Aeronautics and Space Administration under Grant No. NNG04GO70G issued through the Origins of Solar Systems program, and from the Kepler Mission under NASA Cooperative Agreement NCC-1330 with the Smithsonian Astrophysical Observatory. This publication makes use of data products from the Two Micron All Sky Survey, which is a joint project of the University of Massachusetts and the Infrared Processing and Analysis Center/California Institute of Technology, funded by the National Aeronautics and Space Administration and the National Science Foundation.

REFERENCES

Adams, J. D., Stauffer, J. R., Skrutskie, M. F., Monet, D. G., Portegies Zwart, S. F., Janes, K. A., & Beichman, C. A. 2002, AJ, 124, 1570
Alard, C. 2000, A&A, 144, 363
Alard, C., & Lupton, R. H. 1998, ApJ, 503, 325
Alonso, R., et al. 2004, ApJ, 613, L153
An, D., Terndrup, D. M., Pinsonneault, M. H., Paulson, D. B., Hanson, R. B., & Stauffer, J. R. 2007, ApJ, 655, 233
Bakos, G., Noyes, R. W., Kovacs, G., Stanek, K. Z., Sasselov, D. D., & Domsa, I. 2004, PASP, 116, 266
Bakos, G. A. 2006, ApJ, 656, 552
Barnes, J. W., & Fortnoy, J. J. 2004, ApJ, 616, 1193
Burke, C. J., Gaudi, B. S., DePoy, D. L., & Pogge, R. W. 2006, AJ, 132, 210
Burke, C. J., et al. 2007, ApJ, submitted (arXiv:0705.0003)
Cameron, A. C., et al. 2007, MNRAS, 375, 951
Chappelle, R. J., Pinfield, D. J., Steele, I. A., Dobbie, P. D., & Magazzu, A. 2005, MNRAS, 361, 1323
Charbonneau, D., Brown, T. M., Noyes, R. W., & Gilliland, R. L. 2002, ApJ, 568, 377
Charbonneau, D., Brown, T. M., Burrows, A., & Laughlin, G. 2007, in Protostars & Planets V, ed. B. Reipurth, D. Jewitt, & K. Keil (Tucson, AZ: Univ. of Arizona Press), 701
Gaudi, B. S., & Winn, J. N. 2007, ApJ, 655, 550
Guillot, T. 2005, AREPS, 33, 493
Hartman, J. D., Bakos, G., Stanek, K. Z., & Noyes, R. W. 2004, AJ, 128, 1761
Høg, E., et al. 2000, A&A, 355, L27
Jones, B. F., & Stauffer, J. R. 1991, AJ, 102, 1080
Kaluzny, J., Stanek, K. Z., Krockenberger, M., Sasselov, D. D., Tonry, J. L., & Mateo, M. 1998, AJ, 115, 1016
Kovacs, G., Zucker, S., & Mazeh, T. 2002, A&A, 391, 369
Kukarkin, B. V., et al. 1982, New Catalog of Suspected Variable Stars (Moscow: Nauka)
Kurucz, R. L. 1992, IAUS, 149, 225
Latham, D. W. 1992, in IAU Coll. 135, Complementary Approaches to Double and Multiple Star Research, ASP Conf. Ser. 32, ed. H. A. McAlister, & W. I. Hartkopf (San Francisco, CA: ASP), 110
Latham, D. W. 2003, in ASP Conf. Ser. 294, Scientific Frontiers in Research on Extrasolar Planets, ed. D. Deming, & S. Seager (San Francisco, CA: ASP), 409
Latham, D. W. 2007, in ASP Conf. Ser. 366, Transiting Extrasolar Planet Workshop, ed. C. Afonso, D. Weldrake, & Th. Henning (San Francisco, CA: ASP)
Mazeh, T., Tamuz, O., & Zucker, S. 2007, ASPC, 366, 119
McCullough, P. R., Stys, J. E., Valenti, J. A., Fleming, S. W., Janes, K. A., & Heasley, J. N. 2005, PASP, 117, 783
McCullough, P. R., et al. 2006, ApJ, 648, 1228
O'Donovan, F. T., et al. 2006, ApJ, 651L, 61
O'Donovan, F. T., et al. 2007, ApJ, 663L, 37
Pepper, J., Pogge, R. W., & Depoy, D. L. 2003, Acta Astron., 53, 213
Pepper, J., et al. 2007, PASP, 119, 923
Pollacco, D. L., et al. 2006, PASP, 118, 1407
Samus, N. N., & Durlevich, O. V. 2004, Combined General Catalog of Variable Stars (ed. 4.2; Moscow: Sternberg Astron. Inst.)
Schlegel, D. J., Finkbeiner, D. P., & Davis, M. 1998, ApJ, 500, 525
Schwarzenberg-Czerny, A. 1996, ApJ, 460, L107
Skrutskie, M. F. 2006, AJ, 131, 1163
Stetson, P. B. 1987, PASP, 99, 191
Stetson, P. B. 1996, PASP, 108, 851
Tamuz, O., Mazeh, T., & Zucker, S. 2005, MNRAS, 356, 1466
Udalski, A., Pietrzynski, G., Szymanski, M., Kubiak, M., Zebrun, K., Soszynski, I., Szewczyk, O., & Wyrzykowski, L. 2003, Acta Astron., 53, 133
Udalski, A., Szewczyk, O., Zebrun, K., Pietrzynski, G., Szymanski, M., Kubiak, M., Soszynski, I., & Wyrzykowski, L. 2002a, Acta Astron., 52, 317
Udalski, A., Szymanski, M. K., Kubiak, M., Pietrzynski, G., Soszynski, I., Zebrun, K., Szewczyk, O., & Wyrzykowski, L. 2004, Acta Astron., 54, 313
Udalski, A., Zebrun, K., Szymanski, M., Kubiak, M., Soszynski, I., Szewczyk, O., Wyrzykowski, L., & Pietrzynski, G. 2002b, Acta Astron., 52, 1
Udalski, A., et al. 2002c, Acta Astron., 52, 1